

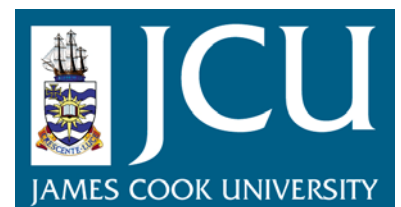
JCU ePrints

This file is part of the following reference:

Villarreal Albitres, William F. (2005)
An experimental investigation into the effect of interface friction on bagasse compaction between grooved steel platens.
Masters (Research) thesis, James Cook University.

Access to this file is available from:

<http://eprints.jcu.edu.au/2113>



An Experimental Investigation into the Effect of Interface Friction on Bagasse Compaction between Grooved Steel Platens

Thesis submitted by

William F. Villarreal Albitres

BE (Mech.), Universidad Nacional de Trujillo, Perú

in May 2005

for the degree of Master of Engineering Science
in the School of Engineering (Mechanical Engineering)
James Cook University

Statement of Access

I, the undersigned, author of this work, understand that James Cook University will make this thesis available for use within the University Library and, via the Australian Digital Theses network or other means, for use elsewhere. All users consulting this thesis will have to sign the following statement:

In consulting this thesis I agree not to copy or closely paraphrase it in whole or in part without the written consent of the author; and to make proper public written acknowledgement for any assistance that I have obtained it

Beyond this, I do not wish to place any restriction on access to this thesis

04 May, 2005

William F. Villarreal A.

Date

Statement of Sources

DECLARATION

I declare that this thesis is my own work and has not been submitted in any other form for another degree or diploma at any university or other institution of tertiary education.

Information derived from the published or unpublished work of others has been acknowledged in the text and a list of reference is given

04 May, 2005

William F. Villarreal A.

Date

Acknowledgements

The author wishes to express his feeling of thankfulness and appreciation to the following people for the valuable help and cooperation given to me during the present investigation work:

My supervisor, Professor Jeffrey G. Loughran, of James Cook University, for suggesting the topic for my investigation, and for his incessant support and guidance throughout the course of my research.

Mr. David Kauppila, whose accurate ideas and suggestions about the experimental part of this investigation led me to be successful in this research project.

The workshop staff, for manufacture of the apparatus. Their ideas and experience with technical materials made the apparatus so practical and effective.

Dr Paul Britton, for the fruitful discussions about compaction and groove angles in a rolling environment.

Drs Gina Curro and George Ridgway, of Learning and Communication, who helped me to have an effective academic writing style.

Finally, to my wife Sara and children Gustavo, Marcelo and Maria-Fernanda, who have supported me and faced my absence with courage, during the two years I undertook this challenge.

Abstract

Modern factory crushing units process prepared sugar cane through sets of counter-rotating grooved rolls. A typical unit in Australia would process in excess of 600 tonnes of material per hour. Throughput and extraction performance is strongly dependent on material behaviour, the geometry and surface condition at the roll bagasse interface. Factories use welding procedures to arc roughen the tips of grooves in an effort to increase friction. Although industry procedures appear ad hoc it is clear that some level of roughness is crucial to performance. A similar statement can be made in respect to roll grooving given the wide variation in adopted practice. This project involved an experimental investigation into the effects of interface friction on bagasse compaction between grooved steel platens. An apparatus was developed for use in the SOE MTS testing facility. A factorial design experiment involving 105 tests randomised in blocks was conducted to discover the interaction between friction (the dependent variable) and groove angle, compaction, and roughness (independent variables). The results indicate that roughness, groove angle and compaction significantly affect friction coefficient. While roughness and groove angle contribute to increase friction coefficient, compaction causes a marked decrease. Observations on samples of bagasse exhibiting pure shear suggest that the frictional forces generated at the interface cannot be sustained by the shear strength of bagasse. Comparisons between friction coefficient and shear coefficient showed that the friction coefficient values approach the shear coefficient values under particular geometric and loading conditions. An empirical model was developed to explore variables. The effect of groove angle, degree of roughness (location and size of roughened asperity) and sample compaction on friction has been ascertained.

Contents

| | |
|--|-----------|
| Statement of access | ii |
| Statement of sources | iii |
| Acknowledgments | iv |
| Abstract | v |
| Contents | vi |
| Table | x |
| Figures | xi |
| Symbols | xvi |
| 1 Introduction | 1 |
| 1.1 Overview..... | 2 |
| 1.2 Description of the rolling process | 3 |
| 1.3 Grip and deformation of bagasse by grooved rollers | 4 |
| 1.4 Contact mechanism between surfaces | 4 |
| 1.5 The necessity of friction | 6 |
| 1.6 Statement of the problem | 6 |
| 1.7 The significance of this research | 8 |
| 1.7.1 The requirement for the sugar industry | 8 |
| 1.7.2 The requirement for computational and experimental modelling of the cane crushing | 9 |
| 1.8 Thesis objectives | 9 |
| 1.9 Thesis outline | 10 |
| 2 Literature review | 12 |
| 2.1 The physical structure of prepared sugar cane and bagasse | 13 |
| 2.1.1 The nature of prepared cane | 13 |
| 2.1.2 The nature of bagasse | 14 |
| 2.2 The basic physical properties of bagasse | 15 |
| 2.3 Friction theory | 17 |
| 2.3.1 The classical definition of friction | 17 |
| 2.3.2 A description of contact area between two bodies A and B..... | 19 |
| 2.3.3 The concept of friction angle | 22 |
| 2.3.4 Sliding friction | 23 |

| | |
|---|-----------|
| | vii |
| 2.4 Friction in a rolling environment | 24 |
| 2.4.1 The bagasse compression mechanism | 24 |
| 2.4.2 Contact between fibrous material and grooved roller | 25 |
| 2.4.3 Frictional stress at the interface between bagasse and roller | 26 |
| 2.4.4 Failure criterion at an interface plane | 28 |
| 2.4.5 Drucker-Prager/Cap (DPC) plasticity model | 30 |
| 2.4.6 Coulomb wedge analysis | 32 |
| 2.4.7 Reaction forces in grooved elements subjected to compressive load | 34 |
| 2.4.8 The friction coefficient value on a grooved surface | 36 |
| 2.5 The texture of the contact surface between bagasse and a grooved platen | 38 |
| 2.5.1 Quantification of hard-facing roughness on a grooved surface | 41 |
| 2.6 Dimensional analysis for friction coefficient between bagasse and a rolling surface | 42 |
| Summary | 51 |
| 3 Literature review on experimental investigations | 52 |
| 3.1 Introduction | 53 |
| Summary | 58 |
| 4 Research methodology | 59 |
| 4.1 Description of the samples | 60 |
| 4.1.1 Weight and number of samples | 60 |
| 4.1.2 Collection of samples | 61 |
| 4.2 Experimental apparatus and instrumentation | 61 |
| 4.2.1 The shear box | 61 |
| 4.2.2 The platens | 62 |
| 4.3 Description of the experiment | 65 |
| 4.3.1 The variables | 65 |
| 4.3.2 The experimental procedure | 67 |
| 4.3.3 Experimental design | 69 |
| 4.3.4 Analytical model describing the experiment | 70 |
| 4.3.5 Design of the experimental model | 70 |
| 4.3.6 Boundary conditions and restriction for the experiments | 72 |
| 4.3.7 Collection of the experimental data | 73 |
| 4.4 Research hypothesis | 74 |
| 4.5 Statistical technique of evaluation | 74 |

| | |
|---|------------|
| | viii |
| 4.5.1 The empirical model | 75 |
| 4.5.2 The best response curve | 76 |
| Summary | 80 |
| 5 Results | 81 |
| 5.1 The response of the friction coefficient value to roughness, groove angle and compaction | 82 |
| 5.2 The friction coefficient model | 87 |
| 5.3 Optimization of the friction coefficient | 91 |
| 5.4 Bagasse shear failure analysis | 104 |
| 5.5 The influence of liquid in bagasse on the interface friction and shear coefficient values | 107 |
| 5.6 Liquid content in bagasse versus friction coefficient | 108 |
| 5.7 The effect of roughness, compaction and groove angle on bagasse dewatering | 110 |
| Summary | 117 |
| 6 Discussion | 118 |
| 6.1 The response of the friction coefficient to roughness, groove angle, and compaction | 119 |
| 6.2 The maximisation of the friction coefficient | 127 |
| 6.3 The dewatering of bagasse | 127 |
| Summary | 129 |
| 7 Conclusions | 130 |
| 7.1 Future investigations | 132 |
| References | 133 |
| Appendices | 139 |
| Appendix A Example of calculations | 140 |
| Appendix B Calculation of samples | 146 |
| Appendix C Shear box design | 148 |
| Appendix D Set of steel grooved platens used for the experiments..... | 150 |
| Appendix E Miscellanea | 151 |
| Appendix F Laboratory measurements..... | 155 |

Tables

| | | |
|------------|---|-----|
| Table 2.1 | Relation of relevant variables involved at the interface friction between bagasse and roller | 46 |
| Table 4.1 | Average values of constituents parameters of bagasse used during the tests | 60 |
| Table 4.2 | Main characteristics of the platens used during the tests | 63 |
| Table 4.3 | Variable measurements and instrumentation applied | 64 |
| Table 4.4 | Levels selected for each variable and its measurement units | 66 |
| Table 4.5 | Measurement errors of main parameters to measure shear forces | 67 |
| Table 4.6 | Mass of bagasse used for the tests as a function of compaction at different groove angles | 68 |
| Table 4.7 | Randomised order of the samples for the split-split-plot design for shear force tests on steel groove platens | 73 |
| Table 4.8 | Analysis of variance for 3x3x4 factorial | 76 |
| Table 4.9 | Code units and level of the variables selected for the experiment design..... | 78 |
| Table 4.10 | The Box-Behnken design for the three variables at two replicates..... | 79 |
| Table 5.1 | Friction coefficient results between bagasse and grooved steel platens | 83 |
| Table 5.2 | Analysis of variance for friction coefficient under roughness, groove angle and compaction factors | 86 |
| Table 5.3 | Comparisons among levels within each factor tested which caused a greater friction coefficient..... | 87 |
| Table 5.4 | Experimental and predicted value for the friction coefficient | 88 |
| Table 5.5 | ANOVA for response surface cubic model | 90 |
| Table 5.6 | Data for the shear coefficient at three compaction levels | 106 |
| Table 5.7 | Analysis of variance for the shear coefficient | 106 |
| Table 5.8 | Data for shear coefficient under the combined effect of compaction and moisture | 107 |
| Table 5.9 | Analysis of variance for the shear coefficient versus compaction and moisture | 108 |

| | | |
|------------|--|-----|
| Table 5.10 | Results for the friction coefficient, by combining moisture, groove angle and compaction, holding 2.25 mm average roughness | 109 |
| Table 5.11 | Analysis of variance for the friction coefficient versus moisture, groove angle and compaction | 109 |
| Table 5.12 | Data for bagasse dewatering as a function of compaction, roughness, and groove angle | 111 |
| Table 5.13 | The analysis of variance for bagasse dewatering | 112 |
| Table 6.1 | The effect of the variables roughness, groove angle, and compaction on the maximum friction coefficient value | 127 |
| Table 6.2 | The combination for roughness and compaction for predicted maximum friction coefficient at a fixed 35° groove angle | 128 |
| Table 6.3 | Comparison in percentages of extracted liquid between 35° and 100° groove angles at three compaction levels, at 52% moisture bagasse | 128 |
| Table B.1 | The friction coefficients values for four variables reported by Cullen (1965) | 146 |
| Table B.2 | Statistical parameters to calculate the number of samples | 147 |

Figures

| | | |
|-------------|--|----|
| Figure 1.1 | Typical arrangement of a roughened six-roll mill of a crushing unit | 3 |
| Figure 1.2 | Aspect of the interface friction between grooved surfaces (after, Kauppila, 2003) | 5 |
| Figure 2.1 | Microscopic view of a vascular bundle in a sugar cane stem (Gamble, 2003) | 14 |
| Figure 2.2 | Magnification of a fibre element and its surface texture | 15 |
| Figure 2.3 | Mass-volume components of a prepared cane or bagasse sample: (a) prior to juice expression at $t = 0$; (b) at any time during a compression test (Leitch, 1996) | 15 |
| Figure 2.4 | Reacting force generated at the interface of two bodies due to a force applied to one of them (Blencoe & Williams, 1997) | 19 |
| Figure 2.5 | Real contact areas of two bodies before and after the action of a compressive load | 19 |
| Figure 2.6 | Diversity of friction coefficients values for different materials (Ludema, 1996) | 21 |
| Figure 2.7 | Definition of friction angle | 23 |
| Figure 2.8 | Compression process between fibrous material and a pair of rollers | 25 |
| Figure 2.9 | Potential void reduction of bagasse between grooved surfaces (after Briton, 2001) | 25 |
| Figure 2.10 | Frictional forces acting in a rolling environment. A mean roller diameter is assumed | 26 |
| Figure 2.11 | Schematic showing a plane strain view of two roughened rollers | 27 |
| Figure 2.12 | Equilibrium of forces on grooved roller surfaces | 28 |
| Figure 2.13 | Potential failure planes of a material subjected to shear stress..... | 29 |
| Figure 2.14 | A family of conventional DPC yield limits for different levels of relative density | 31 |
| Figure 2.15 | The non-conventional DPC model parameters including a family of DPC yield limits for different levels of bagasse compaction (relative densities) over a range of compression | 32 |

| | |
|-------------|---|
| | xii |
| Figure 2.16 | Failure of a wall due to a normal applied force 33 |
| Figure 2.17 | Free-body diagram of a wedge under a vertical force F 34 |
| Figure 2.18 | Ratio of normal to compressive force versus angle and friction coefficient35 |
| Figure 2.19 | Distribution of frictional forces on a grooved surface 36 |
| Figure 2.20 | Relationship friction coefficient and groove angle as a function of shear and normal force 37 |
| Figure 2.21 | Components of the contact surface: roughness and waviness making the total profile (Anon., 2001)..... 38 |
| Figure 2.22 | Forms to measure a superficial irregularity: Average roughness, root mean square (rms) 40 |
| Figure 2.23 | Surface profiles with different shapes, but similar average roughness value (Anon. 2001) 40 |
| Figure 2.24 | Average roughness, R_a , for a grooved surface covered with asperities 41 |
| Figure 2.25 | Dimensional set matrix for friction coefficient composed of ten dimensionless variables 47 |
| Figure 2.26 | Contact of roughened area as a function of bagasse penetration 49 |
| Figure 3.1 | Limiting friction coefficient for different normal pressures for fresh prepared cane (Adam, 2004) 55 |
| Figure 3.2 | Friction coefficient versus groove angle for various speeds at low and high normal pressure (Adam, 2004) 55 |
| Figure 3.3 | Friction coefficient versus rubbing speed for flat and grooved surfaces at low and high speed (Adam, 2004) 56 |
| Figure 3.4 | Forces acting on an element of material in a roller groove (Adam, 2004)... 57 |
| Figure 4.1 | Shear box used for the experiment to determine shear forces..... 62 |
| Figure 4.2 | Fibre machine, apparatus for determining the fibre in bagasse (after Loughran et., al , 1988) 64 |
| Figure 4.3 | MTS machine for uniaxial compression tests 65 |
| Figure 4.4 | Diagram of equipments and instrumentation for experimental tests 66 |
| Figure 5.1 | The effect of roughness, groove angle and compaction on the mean value of the friction coefficient83 |
| Figure 5.2 | Plots of the friction mean friction coefficient value for roughness, groove angle, and compaction , at three-way interaction..... 85 |
| Figure 5.3 | Residual plots for the friction coefficient observations 90 |

| | | |
|-------------|--|-----|
| Figure 5.4 | Comparison between the predictive and experimental values for the friction coefficient | 91 |
| Figure 5.5 | Contour plots for the friction coefficient under a combination of compaction and groove angle with constant roughness..... | 95 |
| Figure 5.6 | Surface plots for the friction coefficient under combination of compaction and groove angle, with constant roughness | 95 |
| Figure 5.7 | Contour plots for the friction coefficient under a combination of compaction and roughness, holding a 35° groove angle | 96 |
| Figure 5.8 | Surface plots for the friction coefficient under a combination of compaction and roughness, holding a 35° groove angle | 96 |
| Figure 5.9 | Contour plots for the friction coefficient under a combination of groove angle and roughness, holding compaction at 400 kg/m ³ | 97 |
| Figure 5.10 | Surface plots for the friction coefficient under a combination of groove angle roughness, holding compaction at 400 kg/m ³ | 97 |
| Figure 5.11 | Contour plot for the friction coefficient under the combined effect of groove angle and compaction, holding roughness held at 2.25 mm | 98 |
| Figure 5.12 | Surface plot for the friction coefficient responses under the factors groove angle and compaction, holding roughness at 2.25 mm | 98 |
| Figure 5.13 | Contour plot for of friction coefficient under the combined effect of roughness and compaction, holding a 100° groove angle | 99 |
| Figure 5.14 | Surface plot for the friction coefficient responses under the factors of roughness and compaction, holding 100o groove angle | 99 |
| Figure 5.15 | Contour plots for the friction coefficient under the combined effect of groove angle and compaction, holding compaction 700 kg/m ³ | 100 |
| Figure 5.16 | Surface plot for the friction coefficient responses under the factors of roughness and groove angle, holding compaction at 700 kg/m ³ | 100 |
| Figure 5.17 | Contour plot for the friction coefficient value versus compaction and groove angle, holding average roughness at 4.50 mm | 101 |
| Figure 5.18 | Surface plot for the friction coefficient responses versus compaction and groove angle, holding average roughness at 4.50 mm | 101 |
| Figure 5.19 | Contour plots for the friction coefficient value under the combined effect of roughness and compaction, holding 180° groove angle | 102 |
| Figure 5.20 | Surface plot for the friction coefficient value under the conditions of roughness and compaction, holding groove angle at 180° | 102 |

| | | |
|-------------|---|-----|
| Figure 5.21 | Contour plots for the friction coefficient value under the combined effect of groove angle and roughness, holding compaction at 1000 kg/m ³ | 103 |
| Figure 5.22 | Surface plot for the friction coefficient response versus groove angle and roughness, holding compaction 1000 kg/m ³ | 103 |
| Figure 5.23 | Shear and friction coefficients as a function of the compaction at different groove angles and roughness of surface..... | 104 |
| Figure 5.24 | Shear and friction coefficient versus normal force at different groove angles and roughness | 105 |
| Figure 5.25 | Shear and friction coefficient measurements: (a) shear test without scraper; (b) friction coefficient test using scraper to avoid internal shear failure ... | 106 |
| Figure 5.26 | Comparison of shear coefficient at two different levels of bagasse moisture as a function of compaction | 108 |
| Figure 5.27 | Friction coefficient values versus bagasse moisture and groove angle..... | 110 |
| Figure 5.28 | Friction coefficient values versus bagasse moisture and compaction..... | 110 |
| Figure 5.29 | Profile plots for extracted liquid versus roughness, groove angle and compaction | 113 |
| Figure 5.30 | Interaction plots for extracted liquid and roughness, groove angle, and compaction effects..... | 113 |
| Figure 5.31 | Contour plots of extraction versus roughness and compaction | 114 |
| Figure 5.32 | Surface plot of extraction versus compaction and roughness | 114 |
| Figure 5.33 | Contour plots of extraction versus roughness and groove angle | 115 |
| Figure 5.34 | Surface plot of extraction versus roughness and groove angle | 115 |
| Figure 5.35 | Contour plots of extraction versus compaction and groove angle. | 116 |
| Figure 5.36 | Surface plot of extraction versus compaction and groove angle | 116 |
| Figure 6.1 | Traces left by asperities on bagasse after contacting a roughened steel flat platen at 1000 kg/m ³ compaction | 119 |
| Figure 6.2 | Evidence of the shear failure of bagasse after having been pushed 14 mm | 120 |
| Figure 6.3 | The internal friction coefficient of the bagasse as a function of filling ratio (referred to density fibre = 1530 kg/m ³) | 121 |
| Figure 6.4 | The friction coefficient tests at 1000 kg/m ³ compaction, 60° groove angle, and 2.25 mm average roughness. Slippage seems to occur outside the interface | 121 |

| | | |
|-------------|---|-----|
| Figure 6.5 | The friction coefficient test at 1000 kg/m ³ compaction, 180° groove angle, and 2.25 mm average roughness. Potential slippage occurring outside the interface | 122 |
| Figure 6.6 | A typical example of material subjected to direct shear (Atkinson, 2002) | 122 |
| Figure 6.7 | A schematic diagram of friction mechanism: (a) shear stress rises with the increment of normal pressure. (b) Plastic flow alternated with ploughing. (c) Shear stress remains constant, μ decreases with increasing normal pressure | 123 |
| Figure 6.8 | (a) Aligned appearance of fibres under 1000 kg/m ³ compaction, smooth, 100° groove angle. (b) Randomised appearance of fibre under 400 kg/m ³ compaction, 2.25 mm height of asperity, and 35° groove angle | 124 |
| Figure 6.9 | A comparison of friction coefficients with respect to Cullen (1965)..... | 125 |
| Figure 6.10 | Relation shear/friction coefficient compared to the results of Cullen (1965) and Plaza (1997) | 126 |
| Figure D.1 | Set of smooth steel grooved platens. Roughness assumed zero | 150 |
| Figure D.2 | Set of roughened steel grooved platens with 2.25 average asperities | 150 |
| Figure D.3 | Set of roughened steel grooved platens with 4.50 average nodules | 150 |
| Figure E.1 | Bagasse compacted at 35° groove angle at different levels: (a) 1000 kg/m ³ and (b) 700 kg/m ³ | 151 |
| Figure E.2 | Groove platens roughened by nodules. Fibre forming a curvature radius around the nodule; (a) 60° and (b) 35° | 152 |
| Figure E.3 | (a) Traces of the nodules indented in bagasse without signs of causing ploughing. (b) Platen roughened with nodules after being pushed about 14 mm | 152 |
| Figure E.4 | (a) Flat smooth platen pushed at 1000 kg/m ³ . (b) Flat roughened platen pushed at 700 kg/m ³ | 153 |
| Figure E.5 | (a) Flat platen with nodules pushed at 1000 kg/m ³ . (b) Platen with asperities showing fibre attached around the roughened flank of the tooth | 153 |
| Figure E.6 | (a) Roughened platen after having taken the bagasse out. (b) Shear test for internal shear coefficient. Test run without scraper | 154 |
| Figure E.7 | Mass of bagasse fixed. Platen pushed to cause shear stress at the interface friction. (a) smooth surface, 35°, 1000 kg/m ³ ; (b) smooth surface, 100°, 700 kg/m ³ | 154 |

Symbols

| | |
|------------|---|
| A | Cross-sectional area |
| A_a | Apparent area |
| A_t | true area |
| C | Variable compaction |
| C_c | Compression ratio |
| C_f | Filling ratio |
| D | Roller diameter |
| D_m | Mean Diameter |
| E | Elastic modules |
| F | Force |
| F_c | Compressive force, yield function in cap region |
| F_n | Normal force |
| FR | filling ratio |
| F_s | Yield function in Drucker-Prager shear region |
| F_t | Tangential force, yield function in transition region |
| G | Variable groove angle |
| G_b | Bagasse shear modules |
| H | Height of bagasse penetration |
| K | Bulk modulus |
| K_o | Plasticity constant |
| L | Length |
| M | Mass |
| N | Reacting normal force |
| N_s | Number of responses |
| N_x, N_y | Reacting normal force components |
| R | Variable roughness, experimental parameter |
| R_a | Average roughness |
| R_q | Root mean square |
| R_x, R_y | Reacting forces components |

| | |
|---------------------|--|
| T | Time |
| V_f | Volume of fibre |
| V_j | Volume of juice |
| V_o | Initial no gas volume of cane |
| W | Gravitational force |
| c | Cohesion coefficient |
| c_w | Cohesion coefficient on the wall |
| d | material cohesion |
| $d_{\tau'}$ | Shear stress differential |
| d_{γ} | Shear strain differential |
| $d_{\sigma'}$ | Normal stress differential |
| d_{ε_v} | Volumetric strain differential |
| $d\tau'$ | Differential of shear strain |
| $d\sigma'$ | Differential of normal stress |
| $\dot{\varepsilon}$ | Shear strain of liquid film |
| f | Fibre fraction |
| f_a | Friction force due to adhesion |
| f_f | Frictional force |
| g | Acceleration due to gravity |
| h | Height of asperity |
| h_d | Hardness |
| h_m | Height of bagasse blanket |
| i | initial condition |
| k | Number of levels |
| m_f | Final mass of prepared cane or bagasse |
| m_i | Initial mass of prepared cane or bagasse |
| p | Hydrostatic pressure |
| q | Von Mises equivalent stress |
| s_t | Tangential speed |
| v | Peripheral speed |
| w | Work opening |
| α | Angle of nip, cap transition parameter |

| | |
|--------------------------------------|--|
| α_a | Asperity angle |
| α_i | Initial contact angle |
| \hat{a} | Treatment number |
| β | Neutral plane angle, internal friction coefficient |
| λ | Specific density |
| γ | Compaction |
| γ_{bss} | Bagasse shear strain |
| γ_{zx} | Engineer's strain |
| $\dot{\gamma}_f$ | Liquid film shear strain |
| δ | Displacement differential |
| ε_e | Elastic strain |
| ε_p | Plastic strain |
| ε_v | Volumetric strain |
| $\varepsilon_{xz}, \varepsilon_{zx}$ | Pure shear strain |
| ζ | Asperity tip radius |
| η | Angle of an inclined wall |
| θ | Groove angle |
| θ_s | Shear plane angle |
| μ | Friction coefficient |
| μ_{pp} | Porous pressure |
| μ_s | Static friction |
| μ_w | Friction coefficient on the wall |
| v | Specific volume |
| π | Dimensional product |
| ρ_c | Density of cane |
| ρ_f | Density of fibre |
| ρ_j | Density of juice |
| ρ_o | No gas density of prepared cane |
| σ | Total normal stress |

| | |
|--------------------------------|--|
| σ' | Normal effective stress |
| σ_Y | Yield stress |
| $\sigma_x, \sigma_y, \sigma_z$ | Normal stress components |
| $\sigma_1, \sigma_2, \sigma_3$ | Normal stress components |
| σ_{sd} | Standard deviation of asperities heights |
| τ, τ' | Shear stress |
| τ_1, τ_2, τ_3 | Shear stress components |
| τ_w | Shear stress on the wall |
| τ_{xy}, τ_{yx} | Internal shear stress |
| ϕ | Angle of friction |
| ϕ_w | Angle of wall |
| ϕ' | Effective angle of internal friction |
| ψ | Plasticity index. |